J Comput Electron (2012) 11:22–28
DOI 10.1007/s10825-012-0389-8

Calculation of phonon spectrum and thermal properties in suspended ⟨100⟩ $In_XGa_{1-X}As$ nanowires

Mehdi Salmani-Jelodar · Abhijeet Paul · Timothy Boykin · Gerhard Klimeck

Published online: 9 February 2012

Abstract The phonon spectra in zinc blende InAs, GaAs and their ternary alloy nanowires (NWs) are computed using an enhanced valence force field (EVFF) model. The physical and thermal properties of these nanowires such as sound velocity, elastic constants, specific heat (C_v), phonon density of states, phonon modes, and the ballistic thermal conductance are explored. The calculated transverse and longitudinal sound velocities in these NWs are ∼25% and 20% smaller compared to the bulk velocities, respectively. The C_v for NWs are about twice as large as the bulk values due to higher surface to volume ratio (SVR) and strong phonon confinement in the nanostructures. The temperature dependent C_v for InAs and GaAs nanowires show a cross-over at 180°K due to higher phonon density in InAs nanowires at lower temperatures. With the phonon spectra and Landauer's model the ballistic thermal conductance is reported for these III–V NWs. The results in this work demonstrate the potential to engineer the thermal behavior of III–V NWs.

Keywords Phonon dispersion relation · Indium gallium arsenide · Nanowire · Specific heat · Thermal conductance

1 Introduction

Low dimensional devices especially nanowires received considerable attention due to their potential applications in different areas such as nano-electronics and thermoelectricity in the past few years [1, 2]. For many of these applications, thermal properties of nanowires are crucial, both for fundamental understanding of the underlying physics and for the prediction and design in thermoelectric applications. Two different examples illustrate the importance of nanostructure thermal properties: (i) usage of nanowires as heat sinks, where a high thermal conductivity is necessary; (ii) thermoelectric applications such as thermoelectric power generators and coolers [3], where a low thermal conductivity, large Seebeck coefficient and figure of merit (ZT) are required. Measuring thermal properties of semiconductor nanowires on very small-scale devices is a difficult task. This is the main reason for the lack of experimental information on the thermal properties of semiconductor nanowires. Also, most of the measurements have been performed on pure Si and Si/SiGe superlattice nanowires [4, 5]. Recently, some measurements have been reported for InAs nanowires [6, 7]. Also, most theoretical research about phonon spectra and thermal-properties calculations for nanowires are done for Silicon nanowires [4, 8, 9]. A few studies are reported in the III–V material system conducted by molecular dynamics [10, 11]. To compute the thermal properties of materials, the first step is to calculate the phonon dispersion relation. The literature already documents a variety of methods for the calculation of the phonon spectrum, such as the Valence Force Field (VFF) method and its variants [8, 12–15], and *ab initio* based methods [16, 17]. Some of them agree very well with experimentally reported values [8, 15, 17]. In this paper, the enhanced VFF (EVFF) model, which is outlined in [15] is used. The main reasons for using the EVFF model are, (a) it matches very well in crystals, like Si, Ge, and GaAs, where simple VFF potentials are sufficient to match the experimental data [4, 15], and (c) compared to *ab initio* methods, it is less computational

M. Salmani-Jelodar (✉) · A. Paul · G. Klimeck
School of Electrical and Computer Engineering and Network for Computational Nanotechnology, Purdue University, 47907 West Lafayette, USA
e-mail: m.salmani@gmail.com

T. Boykin
Department of Electrical and Computer Engineering, University of Alabama in Huntsville, Huntsville, AL 35899, USA

intensive and enables the atomistic analysis of ultra-scaled structures which are made of a few hundreds/thousands of atoms. The EVFF model [15] is used to compute phonon dispersion relations of zinc blende $In_XGa_{1-X}As$ for arbitrary $X = 0, 0.2, 0.4, 0.6, 0.8$ and 1. Using the phonon dispersion relation, we compute longitudinal and transversal sound velocities (V_{snd}), temperature dependent specific heat (C_v), phonon density of states and ballistic lattice thermal conductance (κ_l). A nanowire with a square cross-section with $6a_0 \times 6a_0$—a_0 is the lattice constant along wire direction (i.e. $\langle 100 \rangle$)—is assumed. This cross-sectional area varies in size slightly due to the alloy composition dependence of a_0 from 3.39 nm to 3.64 nm. The EVFF model's parameter sets for ternary alloys are calculated by using the virtual crystal approximation (VCA). In VCA approach the disorderd $In_XGa_{1-X}As$ alloy would be replaced by an orderd ZAs binary compound. Z is a "pseudoatom" with weighted average properties of Ga and In based on their contribution to the ternary compound [18]. The contents of this paper are organized as follows. In Sect. 2, the EVFF is described briefly along with methods for calculating other thermal properties. In Sect. 3, the computed results are presented with a discussion about them. At the end, in Sect. 4 paper will be concluded.

2 Calculation theory

In this section, the calculation theory is explained briefly. In next sub-section the enhanced Valance Force Field model is introduced briefly. The methodology of the computation for other thermal properties of the lattice is explained in Sect. 2.2. At the end of this section the Landauer model for computing ballistic thermal conductance [19] is explained.

2.1 Enhanced valance force field model

The enhanced VFF [15] is a variant of VFF model, which is a force constant based atomic potential (U) calculation approach. The simplest and most widely used approach of the VFF model is due to Keating [14], together with anharmonic corrections [20], has been shown to provide reasonable agreement with the experiment when it comes to the modeling of electronic states in strained nanostructures [21]. Yet, it is well known that it fails to reproduce basic bulk properties of zinc blende crystals [15].

The enhanced VFF model is similar to the model by Kane [22], but includes stretch-bend and third-order stretching nearest-neighbor terms instead of a second-nearest neighbor stretch term. This model has 5 different types of force constants, which represent the various kinds of interaction between the atoms. These force constants are as follows, (a) bond-stretching (α), (b) bond-bending (β), (c) stretch-bend interactions (γ), (d) cross-stretch interactions (δ) and (e) co-planar bond-bend interactions (λ). The first two terms are from the original Keating model [8, 14], which are not sufficient to reproduce the bulk phonon dispersion accurately in zinc blende semiconductors [15]. Hence, higher order interactions are included in the original Keating VFF model. The motion of atoms in the semiconductor structure is captured by a dynamical matrix (DM). The DM is assembled using the second derivative (Hessian) of the crystal potential energy (U). The bulk DM has periodic boundary conditions along all directions (Born-von Karman condition) due to the assumed infinite material extent in all directions. For suspended $\langle 100 \rangle$ NWs, periodic boundary conditions are applied only along the length of the wire (X-axis) assuming an infinitely long wire, whereas the surface atoms (Y–Z axis) are free to vibrate [8].

2.2 Lattice property calculations

Other properties can be extracted from the phonon spectrum of solids. The descriptions of the several important ones are described below:

2.2.1 *Sound velocity*

The sound velocity in the solid is an important crystal parameter. The sound velocity (V_{snd}) is the group velocity (V_{grp}) of the acoustical branches near the center of Brillouin Zone (BZ) (for $q \to 0$). According to the acoustic modes used for the calculation of V_{grp}, the sound velocity can be either (a) longitudinal ($V_{snd,l}$) or (b) transverse ($V_{snd,t}$). Then, V_{snd} in a material is given by:

$$V_{snd} = \left.\frac{\partial \omega(q)}{\partial q}\right|_{q \to 0} \tag{1}$$

where, q is wave vector and $\omega(q)$ is the frequency of the acoustical branch at q.

2.2.2 *Specific heat*

In a semiconductor structures with two ends are maintained under a small temperature difference, its specific heat (C_v) can be evaluated from the phonon dispersion by [8, 9]:

$$C_v(T) = k_B \sum_{n,q} \left[\frac{(\frac{\hbar\omega(n,q)}{k_B T})^2 \exp(\frac{-\hbar\omega(n,q)}{k_B T})}{1 - \exp(\frac{-\hbar\omega(n,q)}{k_B T})^2} \right], \tag{2}$$

where k_B, $\hbar$, T, n and q are Boltzmann's constant, reduced Planck's constant, mean temperature, number of sub-bands, and phonon wave vector respectively.

2.2.3 Thermal conductance

The temperature dependent lattice thermal conductance (κ_l) in low temperature difference on the contacts can be evaluated from the phonon dispersion using the Landauer's formula for a nanowire conductor by [3, 17, 20, 23]:

$$\kappa_l = \hbar \int_0^{\omega_{\max}} T(\omega) M(\omega) \omega \times \frac{\partial}{\partial T} \left[\left(\exp\left(\frac{\hbar\omega}{k_B T} \right) - 1 \right)^{-1} \right] d\omega \quad (3)$$

where, $T(\omega)$ is the transmission of a phonon mode at a given frequency ω $M(\omega)$ equals the number of phonon sub-bands at frequency ω. At the low temperature limit, it can be approximated $T(\omega) \approx 4 \times T(0)$, since there are four acoustic modes at $\hbar\omega \to 0$, as we will explain in the next section in connection with the discussion about the dispersion relation [17, 24]. In the next section, the results on phonon dispersion and the lattice thermal properties for InGaAs alloy ⟨100⟩ NWs is presented.

3 Results and discussion

3.1 Nanowire structure and parameter set

The structure of nanowires we model is shown in Fig. 1. The EVFF parameter sets (force constants) for InAs and GaAs are listed in Table 1. To find these parameters, the output of the EVFF model is fitted to experimental or *ab initio* reported values. A parallel genetic algorithm was used as an optimization approach to reduce the distance between theoretical model's output and experimental values. The parameterization process is explained in detail in [25]. For target values the experimental and *ab initio* based reported phonon dispersion relation are used [25, 26]. The achieved phonon spectrum, sound velocities and elastic constants from these parameter sets are in very good agreement with experimental values. The phonon dispersion relation for bulk GaAs is shown in Fig. 2.

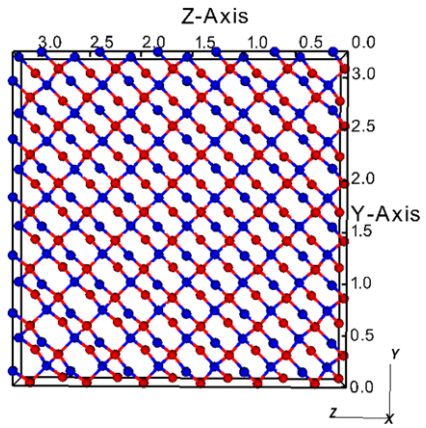

Fig. 1 Above is the structure of square cross-section nanowire without relaxation. The nanowire is confined along Y and Z direction and periodic along X direction. Cross sections view of $\sim 3 \times 3$ nm^2 cross section area wires with orientations ⟨100⟩. The wire is always oriented along the X-axis

3.2 Phonon dispersion relation

The phonon dispersion relation of suspended ⟨100⟩ InGaAs alloy NWs is calculated where the surface atoms were able to vibrate freely. The cross-section size for the nanowire was assumed $6a_0 \times 6a_0$, a_0 being the lattice constant along the wire—which varies from 3.39×3.39 nm^2 in GaAs to 3.64×3.64 nm^2 in InAs. The dispersion relations for all 6 different alloys are depicted in Fig. 3. For each nanowire there are $3N$ sub-bands, with N being the number of atoms in the unit cell. The unit cell is the same as the first slab of the wire along the wire ($1 \times 6 \times 6$). In InGaAs with $6a_0 \times 6a_0$ cross section $N = 288$. Just as in Silicon NWs [8, 28] at low energies, there are four acoustic branches, i.e., one dilatational mode and one torsional mode with linear dispersions, and two flexural ones with quadratic spectra. The many, relatively flat sub-bands starting right above the four acoustic branches originate from the zone-folding of the bulk acoustic branches along the nanowire axis. Many of these flat sub-bands have group velocity close to zero which is a sign for strong phonon confinement in the wire. These phonon dispersions are calculated by NEMO5 [29].

3.3 Thermal properties

3.3.1 Sound velocity

In this sub-section, the sound velocity (V_{snd}) in the nanowire is computed and compared with bulk to see the difference in vibrational modes. V_{snd} is obtained from the slope of third and fourth branches (transverse and longitudinal) around $q \approx 0$ from the phonon dispersion. As it is shown in Fig. 4,

Table 1 The parameter sets for InAs and GaAs EVFF model. X could be Ga or As

Param	α	β(X)	β(As)	γ(X)	γ(As)	δ(X)	δ(As)	ν
GaAs	42.5	7.8	0.01	10.52	−19.98	8.93	−10.55	4.99
InAs	35.03	−0.27	4.13	9.34	−6.24	19.78	−18.49	3.92

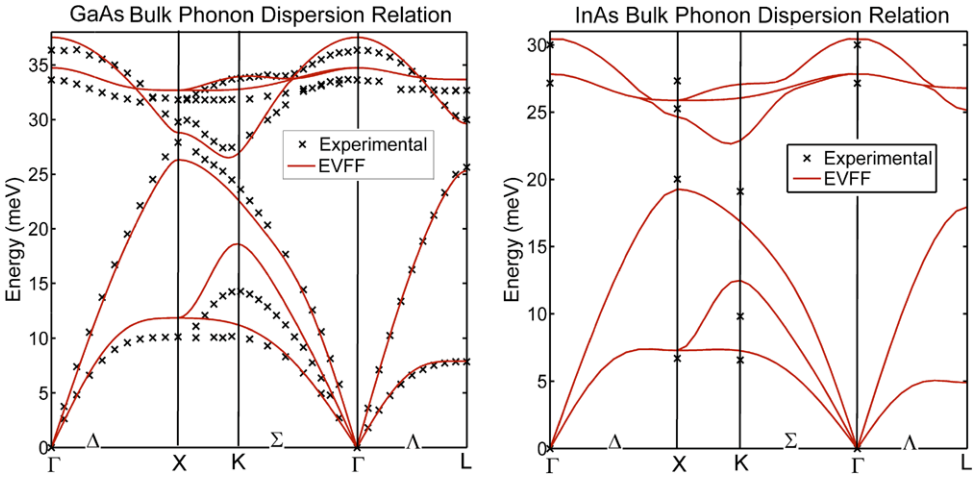

Fig. 2 Phonon spectrum of GaAs (*left*) and InAs (*right*) in bulk are depicted. *The cross points* are experimental values from [26, 27] and *the solid lines* are EVFF's output with listed parameters in Table 1

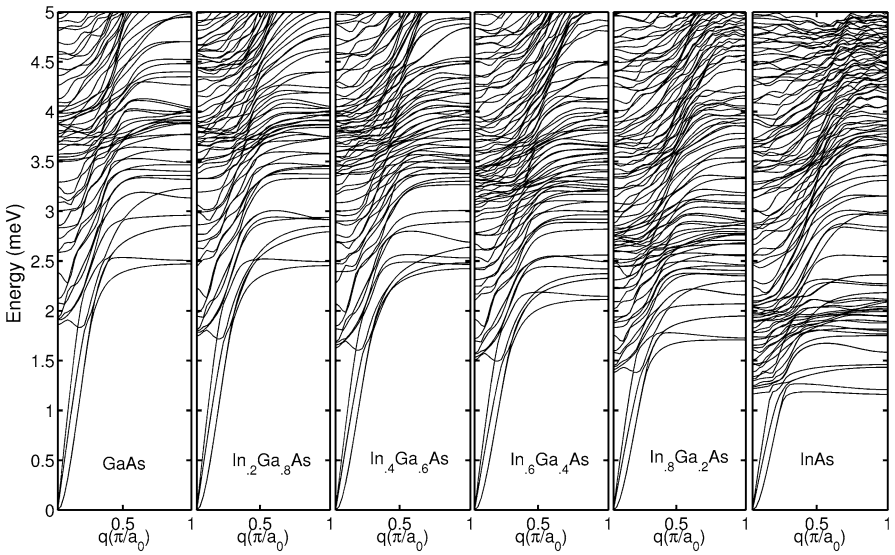

Fig. 3 Low energy branches of phonon band structure for different alloys of InGaAs. The phonon wave vectors, q, are all in the nanowire periodic direction which is ⟨100⟩

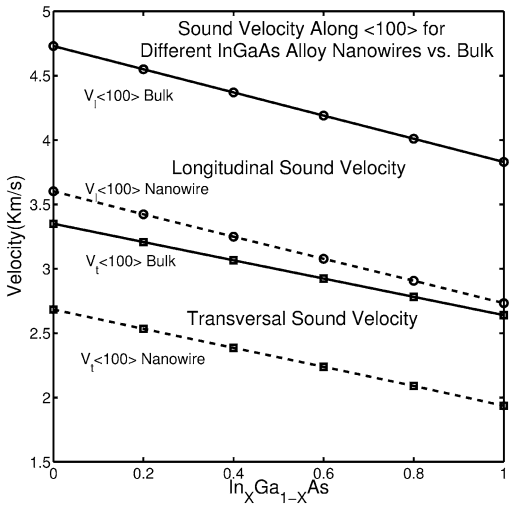

Fig. 4 Longitudinal (V_l) and transversal (V_t) Sound Velocity in ⟨100⟩ InGaAs alloy NWs with freely vibrating transverse boundaries. As a reference the bulk longitudinal and transversal sound velocities are shown along the ⟨100⟩ direction [30]

V_{snd} shows a reduction of about 25% in longitudinal and 20% in transversal modes for NW with respect to bulk InGaAs alloys. The reduced sound velocity in NWs is expected due to acoustical mode softening [28]. This reduction happens since the acoustical bands get flatter in thin nanowires due to phonon confinement. The flattening in acoustical modes also affects other thermal properties because these branches are mainly responsible for the thermal transport. Due to the reduction in sound velocity we can expect a smaller thermal conductance.

3.3.2 *Specific heat*

The specific heat at 300°K of InGaAs nanowires and bulk are show in Fig. 5(left). The specific heat for InGaAs wires are about twice higher than the bulk solids. The main reason for this could be the higher surface to volume ratio (SVR). The other important factor is phonon confinement in small nano-structures [8]. The variation of specific heat (C_v) over

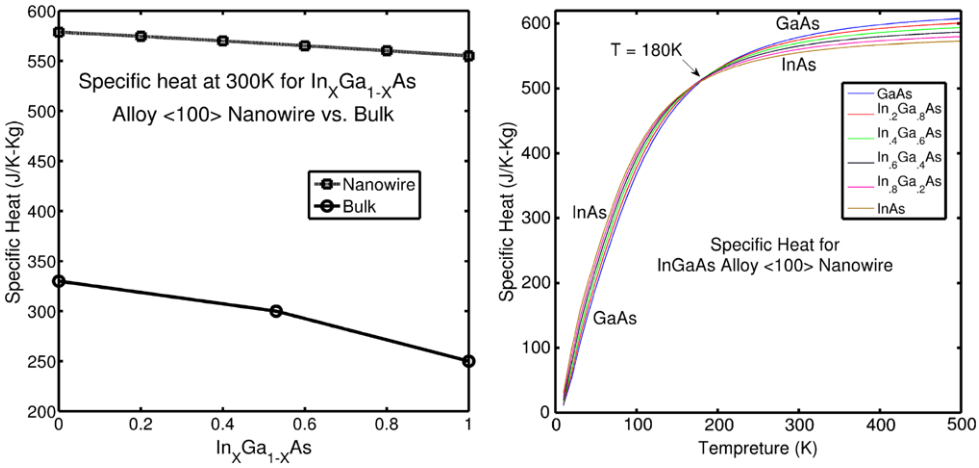

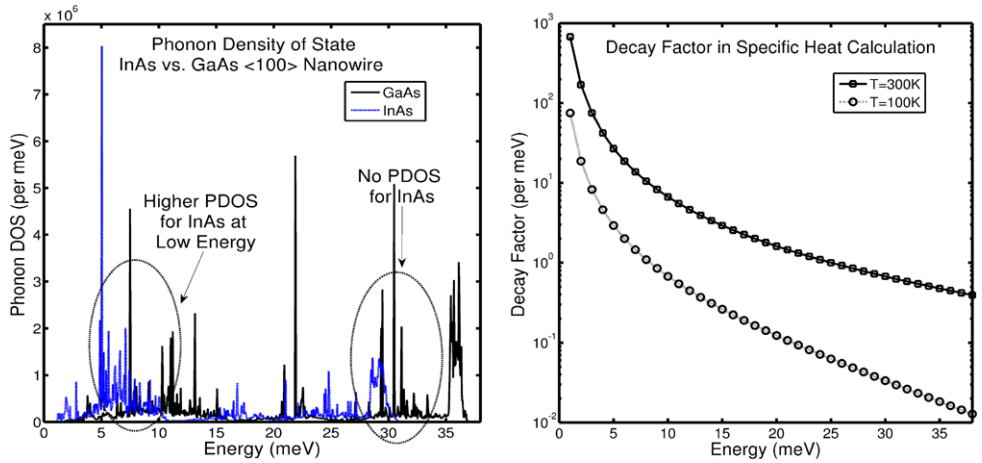

Fig. 5 (*Left*) Variation of the specific heat (C_v) at 300°K in InGaAs alloy nanowires with fraction of In and Ga. As a reference the specific heat for bulk InGaAs [28] is shown by a *black line with holes*. NWs have larger C_v than bulk due to larger surface to volume ratio. (*Right*) the variation of specific heat over temperature for different InGaAs alloy ⟨100⟩NW. These bands cross at temperature 180°K. It is due to different phonon density of states in lower energy points

Fig. 6 (*Left*) The PDOS for InAs and GaAs nanowires are shown. At lower energy the PDOS of InAs is higher than GaAs but in higher energies there is not PDOS for InAs. (*Right*) The decay factor for two different temperatures, 100°K and 300°K, shows the higher PDOS does not have the chance to contribute to the specific heat. Thus, the C_v for InAs in lower energy is higher than GaAs. But at elevated temperatures the GaAs has a higher C_v due to a larger PDOS at higher energy. This causes the crossing point in specific heat branches (Fig. 5)

temperature is shown in Fig. 5(right). There is a crossing point in about 180°K where the specific heat of GaAs exceeds that of InAs. InAs has higher C_v at lower temperatures due to a higher phonon density of states (PDOS). The phonon spectra at low energy show that the InAs curvatures are smaller than those of GaAs, giving a larger PDOS, and suggesting a larger C_v for InAs at lower temperature. There is a direct relation between C_v and PDOS:

$$C_v(T) \propto \mathrm{PDOS}(\omega)\left[\frac{\exp(\frac{-\hbar\omega}{k_B T})}{1-\exp(\frac{-\hbar\omega}{k_B T})^2}\right] \tag{4}$$

where we call the coefficient of PDOS *decay factor* which is the whole—factor after PDOS in the equation. This decay factor and PDOS are depicted in Fig. 6. It is clear in Fig. 6 that the higher phonon states cannot contribute to the specific heat due to the exponential decay factor. Those are the only phonon states contributing to C_v at low temperature where InAs has more states per energy than GaAs. It then follows (strongly since the VCA is used) that if InAs and GaAs specific heat curves cross at $T = 180$°K, all the intermediate alloys must do so at 180°K as well. The phonon density of state and decay factor plot in 100°K and 300°K in Fig. 6 support this claim. The PDOS at a higher energy cannot be occupied in low temperature (e.g., 100°K) but they can contribute in higher temperature (300°K). GaAs has lower PDOS at low energy but higher PDOS at higher energy with respect to InAs which makes its specific heat more than InAs at elevated temperatures. The InGaAs nanowire specific heats are larger than the bulk values at 300°K, which might lead to some confusion with regards to the DuLong-Petit law. The DuLong-Petit law applies only when the temperature is far above the Debye temperature ($T \gg T_\theta$). Here $T_\theta \sim 360$°K (GaAs) [31] or 260°K (InAs) [32] so that for these alloy nanowires $0.8 < T/T_\theta < 1.2$, and clearly DuLong-Petit does not apply.

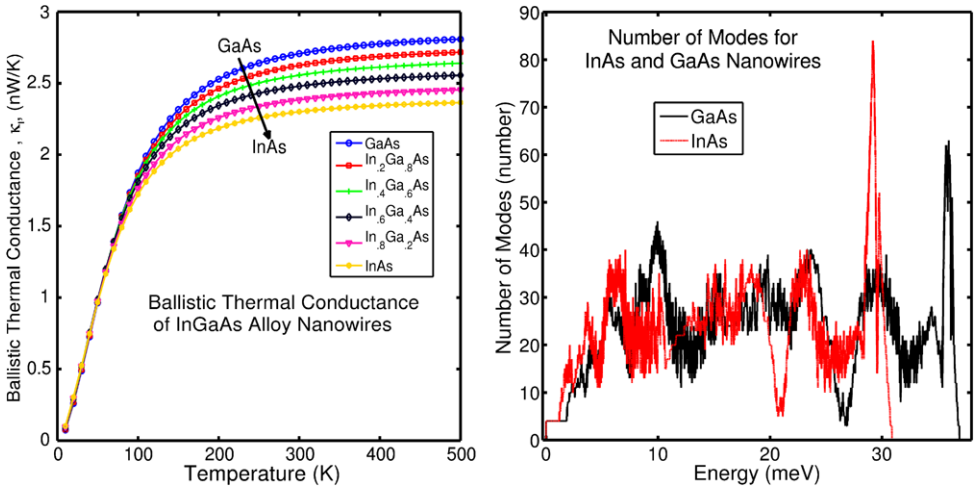

Fig. 7 (*Left*) Temperature dependence of ballistic thermal conductance (κ_l) in variant InGaAs alloy nanowires. GaAs shows the highest thermal conductance and InAs the lowest which is related to higher PDOS and respectively higher number of modes for GaAs. (*Right*) Number of modes for GaAs and InAs nanowire is shown. $M(\omega)$ for GaAs is more spreaded than InAs and covers more area which increases the thermal conductance for GaAs in respect to InAs

3.3.3 Landauer ballistic thermal conductance (κ_l)

To calculate the ballistic thermal conductance (κ_l) the number of modes ($M(\omega)$) should be computed first (see (3)). In these very thin wires surfaces are assumed to be smooth which means there is no surface roughness/scattering, and also the surface structure is incorporated in the phonon modes. In the ideal ballistic limit, all phonon modes propagate through the nanowire with a transmission probability of one. The number of modes is calculated and depicted in Fig. 7(right). Then, the temperature dependent ballistic thermal conductance (κ_l) has been calculated and is shown in Fig. 7(left). The ballistic κ_l increases with temperature. This behavior is due to the increase of the Bose-Einstein distribution at elevated temperatures. In this work we do not consider any kind of scattering (surface roughness, impurity, electron-phonon, and phonon-phonon). Thus, these results represent an ideal upper limit for the ballistic thermal conductance. Consequently, κ_l is expected to decrease further in smaller nanowires due to scattering mechanisms and boundaries which are neglected in the present study.

4 Conclusion

The phonon modes of free-standing $In_XGa_{1-X}As$ alloy ⟨100⟩ nanowires are computed based on an enhanced valance force field phonon model. Using calculated phonon spectrum, transversal and longitudinal sound velocities are derived. The sound velocities in InGaAs ⟨100⟩ wires are 20–25% lower than bulk which is due to flattening of the acoustical branches and phonon confinement in nanowires. Moreover, one finds that specific heat of InGaAs alloy wires increases by elevating the temperature. At low temperatures the InAs wires have a higher specific heat than the GaAs wires. These calculations predict that there will be a crossover around 180°K where the GaAs wires have a higher specific heat compared to the InAs nanowires. The specific heat at 300°K in wires is about twice higher than bulk which is the effect of increase in surface to volume ratio. The surface to volume ratio is an important factor in miniaturization of electronic and thermoelectric devices. At the end, the ballistic thermal conductance was calculated to find out the upper limit for the thermal conductance in InGaAs alloy ⟨100⟩ nanowires. The reported results could be used in nano-electronic and thermoelectric device design.

Acknowledgements The authors would like to thank Dr. Sebastian Steiger, Dr. Michael Povolotskyi and Dr. Denis Areshkin for phonon dispersion calculation code, NEMO5, and useful discussions. This work used nanoHUB.org computational resources operated by the Network for Computational Nanotechnology funded by the National Science Foundation (NSF). Financial support from MSD Focus Center, one of six research centers funded under the Focus Center Research Program (FCRP), a Semiconductor Research Corporation (SRC) entity and by the Nanoelectronics Research Initiative (NRI) through the Midwest Institute for Nanoelectronics Discovery (MIND) are also acknowledged.

References

1. Duan, X., Huang, Y., Cui, Y., Wang, J., Lieber, C., et al.: Indium phosphide nanowires as building blocks for nanoscale electronic and optoelectronic devices. Nature **409**(6816), 66–69 (2001)
2. Persson, A., Björk, M., Jeppesen, S., Wagner, J., Wallenberg, L., Samuelson, L.: InAs-x p x nanowires for device engineering. Nano Lett. **6**(3), 403–407 (2006)
3. Lundstrom, M.: Near-Equilibrium Transport: Fundamentals and Applications. World Scientific, Singapore (2011)
4. Paul, A., Luisier, M., Klimeck, G.: Modified valence force field approach for phonon dispersion: from zinc-blende bulk to nanowires. J. Comput. Electron. (2010)
5. Li, D., Wu, Y., Fan, R., Yang, P., Majumdar, A.: Thermal conductivity of Si/SiGe superlattice nanowires. Appl. Phys. Lett. **83**, 3186 (2003)
6. Persson, A., Koh, Y., Cahill, D., Samuelson, L., Linke, H.: Thermal conductance of InAs nanowire composites. Nano Lett. **9**(12), 4484–4488 (2009)

7. Zhou, F., Moore, A., Bolinsson, J., Persson, A., Fröberg, L., Pettes, M., Kong, H., Rabenberg, L., Caroff, P., Stewart, D., et al.: Thermal conductivity of indium arsenide nanowires with wurtzite and zinc blende phases. Phys. Rev. B **83**(20), 205416 (2011)
8. Paul, A., Luisier, M., Klimeck, G.: Atomistic modeling of the phonon dispersion and lattice properties of free-standing (100) Si nanowires. In: 2010 14th International Workshop on Computational Electronics (IWCE), pp. 1–4. IEEE Press, New York (2010)
9. Zhang, Y., Cao, J., Xiao, Y., Yan, X.: Phonon spectrum and specific heat of silicon nanowires. J. Appl. Phys. **102**, 104303 (2007)
10. Mingo, N., Broido, D.: Lattice thermal conductivity crossovers in semiconductor nanowires. Phys. Rev. Lett. **93**(24), 246106 (2004)
11. Carrete, J., Longo, R., Gallego, L.: Prediction of phonon thermal transport in thin GaAs, InAs and InP nanowires by molecular dynamics simulations: influence of the interatomic potential. Nanotechnology **22**, 185704 (2011)
12. Sui, Z., Herman, I.: Effect of strain on phonons in Si, Ge, and Si/Ge heterostructures. Phys. Rev. B **48**(24), 17938 (1993)
13. Fu, H., Ozoliņš, V., Zunger, A.: Phonons in gap quantum dots. Phys. Rev. B **59**(4), 2881 (1999)
14. Keating, P.: Effect of invariance requirements on the elastic strain energy of crystals with application to the diamond structure. Phys. Rev. **145**(2), 637 (1966)
15. Steiger, S., Salmani-Jelodar, M., Areshkin, D., Paul, A., Kubis, T., Povolotskyi, M., Park, H., Klimeck, G.: Enhanced valence force field model for the lattice properties of gallium arsenide. Phys. Rev. B **84**(15), 155204 (2011)
16. Peelaers, H., Partoens, B., Peeters, F.: Phonon band structure of Si nanowires: a stability analysis. Nano Lett. **9**(1), 107–111 (2008)
17. Markussen, T., Jauho, A., Brandbyge, M.: Heat conductance is strongly anisotropic for pristine silicon nanowires. Nano Lett. **8**(11), 3771–3775 (2008)
18. Grundmann, M.: The Physics of Semiconductors: An Introduction Including Devices and Nanophysics. Springer, Berlin (2006)
19. Landauer, R.: Spatial variation of currents and fields due to localized scatterers in metallic conduction. IBM J. Res. Dev. **1**(3), 223–231 (1957)
20. Lazarenkova, O., Von Allmen, P., Oyafuso, F., Lee, S., Klimeck, G.: An atomistic model for the simulation of acoustic phonons, strain distribution, and grüneisen coefficients in zinc-blende semiconductors. Superlattices Microstruct. **34**(3), 553–556 (2003)
21. Lee, S., Lazarenkova, O., Von Allmen, P., Oyafuso, F., Klimeck, G.: Effect of wetting layers on the strain and electronic structure of InAs self-assembled quantum dots. Phys. Rev. B **70**(12), 125307 (2004)
22. Kane, E.: Phonon spectra of diamond and zinc-blende semiconductors. Phys. Rev. B **31**(12), 7865 (1985)
23. Mingo, N., Yang, L., Li, D., Majumdar, A.: Predicting the thermal conductivity of Si and Ge nanowires. Nano Lett. **3**(12), 1713–1716 (2003)
24. Cleland, A.: Foundations of Nanomechanics: From Solid-State Theory to Device Applications. Springer, Berlin (2003)
25. Salmani-Jelodar, M., Steiger, S., Paul, A., Klimeck, G.: Model development for lattice properties of gallium arsenide using parallel genetic algorithm. In: 2011 IEEE Congress on Evolutionary Computation (CEC), pp. 2429–2435. IEEE Press, New York (2011)
26. Strauch, D., Dorner, B.: Phonon dispersion in GaAs. J. Phys., Condens. Matter **2**, 1457 (1990)
27. Orlova, N.: X-ray thermal diffuse scattering measurements of the [100] and [111] phonon dispersion curves of indium arsenide. Phys. Status Solidi B **93**(2), 503–509 (1979)
28. Thonhauser, T., Mahan, G.: Phonon modes in Si [111] nanowires. Phys. Rev. B **69**(7), 075213 (2004)
29. Steiger, S., Povolotskyi, M., Park, H., Kubis, T., Klimeck, G., et al.: Nemo5: a parallel multiscale nanoelectronics modeling tool. IEEE Trans. Nanotechnol. **10**(6), 1464–1474 (2011)
30. http://www.ioffe.ru/SVA/NSM/Semicond/GaInAs/ (2011)
31. Collaboration: Authors and Editors of the LB Volumes III/17A-22A-41A1b: Gallium arsenide (GaAs), debye temperature, density, heat capacity, melting point. In: Madelung, M.S.O., Rössler, U. (eds.) SpringerMaterials—The Landolt-Börnstein Database. Group IV Elements, IV–IV and III–V Compounds, vol. 41A1b (2011). Part b—Electronic, Transport, Optical and Other Properties. [Online]. Available: http://dx.doi.org/10.1007/10832182_226
32. Collaboration: Authors and Editors of the LB Volumes III/17A-22A-41A1b: Indium arsenide (InAs), debye temperature, density, hardness, melting point. In: Madelung, M.S.O., Rössler, U. (eds.) SpringerMaterials—The Landolt-Börnstein Database (2011). [Online]. Available: http://dx.doi.org/10.1007/10832182_362